Michigan State University

National Superconducting Cyclotron Laboratory

DETECTING MULTIFRAGMENT DISINTEGRATION OF TOROIDAL AND DISK–SHAPED NUCLEAR CONFIGURATIONS.

T. GLASMACHER, C.K. GELBKE, AND S. PRATT.

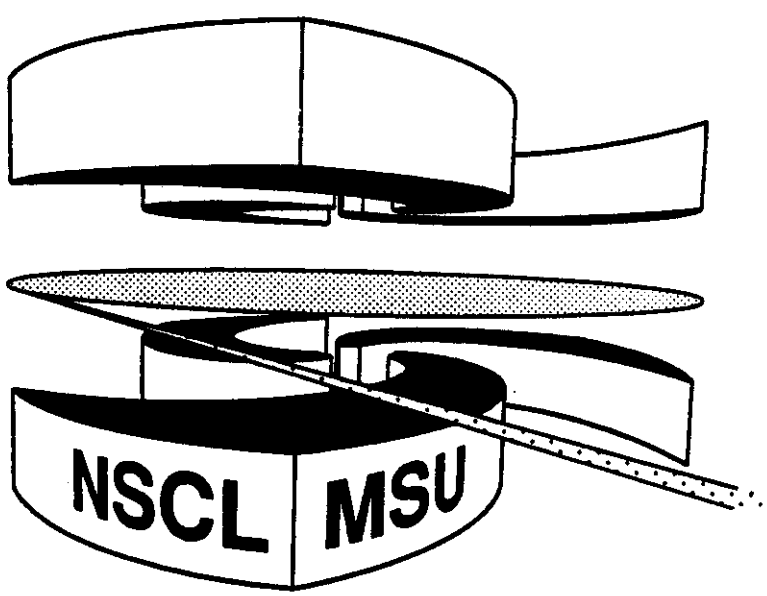

MSUCL-893

JULY 1993

MSUCL-893

Detecting multifragment disintegration of toroidal and disk-shaped nuclear configurations

T. Glasmacher, C.K. Gelbke, and S. Pratt

National Superconducting Cyclotron Laboratory
and Department of Physics and Astronomy,
Michigan State University,
East Lansing, MI 48824, USA

Submitted to Physics Letters B

Abstract

Non-spherical break-up-geometries have been predicted for intermediate-energy heavy-ion collisions. Through studying Coulomb trajectories of the outgoing particles, we show that two-body observables of intermediate mass fragments may contain an experimental signature of a non-spherical breakup configuration.

Microscopic calculations based upon the Boltzmann-Uehling-Uhlenbeck (BUU) transport theory predict [1-4] that ring-, disk- or bubble shaped nuclear configurations may be produced in the aftermath of central collisions between two heavy nuclei at suitably chosen incident energies. These structures are expected to undergo multifragment disintegrations. For example, formation and multifragment breakup of ring-shaped density distributions were predicted [2] for central ($b/b_{max} \leq 0.2$) Nb + Nb collisions at incident energies between $E/A \approx$ 50 and 80 MeV. The existence of such configurations has not yet been confirmed by experimental observation.

A number of single-particle observables were suggested as indicative for the breakup of ring-shaped configurations. For example, arguments based upon the development of Rayleigh-Taylor-like surface instabilities [1] may lead to the qualitative expectation that rings should preferentially break up into fragments of comparable mass. On the other hand, simulations by means of a percolation ansatz [5-7] predict [8] rather unspecific monotonic (power-law or exponential) mass distributions which persist over a broad range of bond-breaking parameters both for ring-shaped and spherically symmetric breakup configurations. In this model, the geometrical configuration of the system does, indeed, influence the exact shape of the mass distribution [5], but this influence is too unspecific to allow a clear distinction between ring-shaped and spherically symmetric breakup configurations. There may also be differences in the low energy portions of the kinetic energy spectra reflecting the different Coulomb barriers of these breakup configurations [2], but these signals can be hard to distinguish from those caused by collective expansion. Most single particle observables depend as much on the breakup dynamics as on the breakup geometry.

Information about the breakup geometry may be derived from two- or many-body observables which depend on the relative location of the emitted particles. Intensity interferometric techniques [9-16] appear particularly promising. Two-proton correlation functions exhibit directional sensitivities [11-14] which could be exploited to distinguish between different geometrical shapes. Unfortunately, protons are emitted already at the very early stages of the reaction for which ring-shaped structures have not yet developed, and a clean signature of the more interesting structures forming at later time scales may be difficult or impossible to extract. Intermediate mass fragments, on the other hand, are believed to preferentially form when the nuclear system has expanded to low density [17-20] for which ring-, disk- or bubble-shaped density distributions have been predicted [1-4]. Observables sensitive to final state interactions between the emerging fragments may, therefore, exhibit sufficient sensitivity to the shape of the breakup configuration. In this paper, we corroborate this qualitative expectation by numerical simulations and show that in favorable cases directional dependences of two-fragment correlation functions can be utilized to distinguish the multifragment breakup of ring- or disk-shaped density distributions from that of spherically symmetric density distributions.

Multifragment disintegrations were simulated for spherical, disk- and ring-shaped source geometries. The particular source geometries discussed in this paper are depicted in Fig. 1. For each geometry, charged particles were randomly distributed into the assumed source volume according to a uniform probability distribution constrained by the requirement that any two particles be separated by more than the sum of their radii, i.e. $r_{ik} > r_0(A_i^{1/3} + A_k^{1/3})$ where A_i and A_k are the mass numbers of fragments i and k and $r_0 = 1.2$ fm. Fragments with elements numbers $1 \le Z \le 20$ were randomly selected according to a power law distribution, $P(Z) \propto Z^{-2.2}$, and the mass numbers were assigned to represent the

most abundant isotope of the corresponding element. The average charge distributed was $Z_{tot} = \sum_{i=1}^{N} Z_i = 74$, corresponding to 90% of the charge of the combined $^{93}Nb + ^{93}Nb$ system.

For each source geometry, the source volume was determined by assuming an average nuclear density of $\rho = 0.3\rho_0$ where ρ_0 denotes the density of normal nuclear matter. The initial velocities of the selected particles were randomly distributed according to a thermal distribution corresponding to a temperature near T=16 MeV. For each event the particles were then shifted into a frame such that their total momentum is zero, $\sum_{i=1}^{N} p_i = 0$; to attain events of comparable breakup energies we discarded events with a total energy that deviated more than 10% from A·9.5 MeV. The assumed element distribution and the temperature parameter are close to those measured [21] for $^{129}Xe + ^{197}Au$ collisions at E/A = 50 MeV. Upon selection of the initial conditions, the system was allowed to disintegrate, and the final fragment momenta were determined by calculating the trajectories of the fragments under the influence of their mutual Coulomb interaction. In these trajectory calculations, the equations of motion were solved by using an adaptive step-size Runge-Kutta algorithm [22]. The integration was terminated when the Coulomb energy between all pairs of particles became smaller than 0.1% of the relative kinetic energy between the same pairs of particles.

Two fragment correlation functions $1+R(v_{red})$ were defined as

$$1 + R(v_{red}) = C \cdot \frac{\sum Y_2(p_1, p_2)}{\sum Y_b(p_1, p_2)}, \qquad (1)$$

where $Y_2(\mathbf{p}_1,\mathbf{p}_2)$ is the calculated two-particle coincidence yield; $Y_b(\mathbf{p}_1,\mathbf{p}_2)$ is the background yield obtained by event mixing [23], i.e. by taking particles 1 and 2 from different events; and v_{red} is the "reduced" relative velocity [16],

$$v_{red} = \frac{v_{rel}}{\sqrt{Z_1 + Z_2}} \qquad (2)$$

which accounts for the scaling of the correlation function for different types of fragments, provided that the Coulomb interaction between the two coincident fragments dominates the shape of the correlation function. This scaling has been shown to persist in an approximate fashion even when the fragments are emitted in the Coulomb field of heavy reaction residues, thus allowing to combine the statistics from different fragment pairs [16]. In Eq. 1, the sums extend over all particle momenta corresponding to a given bin of v_{red} and to other specified cuts - for example the direction of v_{red} or the magnitude and direction of the total momentum $\mathbf{P}=\mathbf{p}_1+\mathbf{p}_2$. The normalization constant C is determined by the normalization condition $\langle R(v_{red})\rangle = 0$ where the average is taken over the interval $0.04\ c \le v_{red} \le 0.05\ c$.

Previous analyses of two-fragment correlation functions explored dependences of $R(v_{red})$ upon the total momentum per nucleon of the emitted fragment pairs and upon event centrality [16,24-26], but the information content of directional dependences was not investigated. These angle integrated two-fragment correlation functions were analyzed by assuming emission from spherical sources, and they revealed [24-26] that multifragment emission in central collisions at $E/A \ge 50$ MeV takes place on a fast time scale ($\tau \le 100$ fm/c).

Correlation functions calculated for the three different break-up geometries, but unconstrained by directional cuts, are presented in Fig. 2. As expected, these correlation functions exhibit little sensitivity to the shape of the emitting system. In our particular example, the ring and disk-shaped configurations are less compact than the spherical configuration. For these less compact systems, the average distance between emitted particles is larger, and the average Coulomb

interaction between the emerging particles is reduced. As a consequence, the minimum of the correlation functions at $v_{red} \approx 0$ is slightly narrower. However, the overall shapes of the correlation functions are very similar. Since the width of the minimum at $v_{red} \approx 0$ depends on the (unknown) size of the emitting system, a distinction of different source shapes by means of such angle integrated correlation functions would be virtually impossible.

Directional dependences of two-fragment correlation functions might provide information about non-spherical breakup configurations. Such directional dependences originate from the Coulomb interaction which acts along the relative coordinate of the two detected particles. Non-isotropic Coulomb correlations may occur classically if the emission sizes are much larger than the Bohr radii of the coincident fragment pairs. This condition is well satisfied for intermediate mass fragments; for example, the Li + Li Bohr radius is 1 fm.

The two-body origin of such directional dependences and their possible attenuation due to final-state interactions with other emitted particles are illustrated in Fig. 3, for the case of emission from a ring-shaped distribution. The figure shows parallel and transverse correlation functions, as defined below, calculated by neglecting all final-state interactions with the exception of that between the detected fragment pairs (Fig. 3a) and, alternatively, by taking the Coulomb interaction between all emitted fragments into account (Fig. 3b). The directional cuts applied in the evaluation of the correlation functions were defined in terms of the angle between the relative fragment velocity ($\hat{\mathbf{v}}_{rel} = \mathbf{v}_{rel}/|\mathbf{v}_{rel}|$) and the symmetry ($\hat{\mathbf{z}}$) axis. Correlation functions with the relative velocity of the two fragments parallel ($|\hat{\mathbf{v}}_{rel} \cdot \hat{\mathbf{z}}| \geq 0.75$) and transverse ($|\hat{\mathbf{v}}_{rel} \cdot \hat{\mathbf{z}}| \leq 0.25$) to the symmetry axis have different shapes, with the transverse

correlation function rising more gradually towards $1+R(v_{red}) = 1$ than the parallel correlation function. This difference is most pronounced when final-state Coulomb interactions with other emitted particles can be neglected (Fig. 3a); it becomes attenuated by final state interactions with the remaining system (Fig. 3b).

While distortions due to n-body interactions are difficult to understand without resorting to trajectory calculations, one should expect these to be most pronounced when particles are detected in directions which correspond to emission from regions of strongly diverging electric field lines. For ring- and disk-shaped charge distributions, these regions of strongly diverging field lines are located at the rims of the rings and disks. Hence, distortions should be largest, when particles are emitted from the rims, i.e. when they are detected in a direction perpendicular to the symmetry axis. Distortions should be less pronounced when the fragments are detected along the symmetry axis. Further, distortions due to final-state interactions with the source should be smaller for particles of higher velocity. Since, for thermal emission, light fragments have larger velocities than heavy fragments, one may expect to improve the sensitivity to directional cuts by restricting the analysis to lighter fragments. These qualitative expectations are supported by results of our many-body trajectory calculations [27]. The difference between parallel and transverse correlation functions can, indeed, be enhanced by selecting lighter fragments which are preferentially emitted in the direction of the symmetry axis.

Figure 4 illustrates the sensitivity of parallel ($|\hat{v}_{rel} \cdot \hat{z}| \geq 0.75$) and transverse ($|\hat{v}_{rel} \cdot \hat{z}| \leq 0.25$) correlation functions to the source geometry. Only lighter fragments ($3 \leq Z \leq 8$) were used in this analysis, and emission along the symmetry axis was enhanced by the cut $|\hat{\mathbf{P}} \cdot \hat{\mathbf{z}}| \geq 0.75$, where $\hat{\mathbf{P}} = \mathbf{P}/|\mathbf{P}|$.is the unit

vector along the direction of the total momentum, $\mathbf{P} = \mathbf{p}_1 + \mathbf{p}_2$, of the two detected fragments. For spherical sources of negligible lifetime, parallel and transverse correlation functions are, as expected, very similar, see Fig. 4a. (Some minor differences may be caused by final-state interactions with other particles.) Ring- and disk-shaped distributions, on the other hand, produce rather different parallel and transverse correlation functions, an effect which can be measured without much difficulty. This qualitative difference is sensitive to the shape of the source. It allows a clear distinction of spherical sources from ring- and disk-shaped sources, but it does not provide a distinction between ring- and disk-shaped geometries. Such more subtle differences in source geometries appear to be very difficult to establish by experimental observation.

This work was supported by the National Science Foundation under Grants PHY-9214992, PHY-925355, and PHY-9017077.

References

1. L. G. Moretto et al., Phys. Rev. Lett. 69 (1992) 1884.
2. W. Bauer, G. F. Bertsch, and H. Schulz, Phys. Rev. Lett. 69 (1992) 1888.
3. D.H.E. Gross, B.A. Li, and A.R. DeAngelis, Ann. Physik 1 (1992) 467.
4. B. Borderie, B. Remaud, M.F. Rivet, and F. Sebille, Phys. Lett. B302 (1993) 15.
5. W. Bauer, D.R. Dean, U. Mosel, and U. Post, Phys. Lett. 150B (1985) 53.
6. W. Bauer, U. Post, D.R. Dean and U. Mosel, Nucl. Phys. A452 (1986) 699.
7. W. Bauer, Phys. Rev. C38 (1988) 1297.
8. L. Phair, W. Bauer, and C. K. Gelbke, Preprint MSUCL-890 (1993).
9. S.E. Koonin, Phys. Lett. B70 (1977) 43.
10. D.H. Boal, C.K. Gelbke, and B.K. Jennings, Rev. Mod. Phys. 62 (1991) 14.
11. S. Pratt and M.B. Tsang, Phys. Rev. C36 (1987) 2390.
12. T.C. Awes et al., Phys. Rev. Lett. 61 (1988) 2665.
13. G.F. Bertsch, Nucl. Phys. A498 (1989) 173c.
14. W.G. Gong, W. Bauer, C.K. Gelbke, and S. Pratt, Phys. Rev. C43 (1991) 781.
15. W. Bauer, C.K. Gelbke, and S. Pratt, Ann. Rev. Nucl. Part. Sci. 42 (1992) 77 .
16. Y.D. Kim et al., Phys. Rev. C45 (1992) 387 .
17. W.A. Friedman, Phys. Rev. Lett. 60 (1988) 2125 ; Phys. Rev. C42 (1990) 667.
18. D.R. Bowman et al., Phys. Rev. Lett. 67 (1991) 1527.
19. R.T. de Souza et al., Phys. Lett. B268 (1991) 6.
20. K. Hagel et al., Phys. Rev. Lett. 2141 (1992) 2141.
21. D.R. Bowman et al., Phys. Rev. C46 (1992) 1834.
22. W. H. Press et al., Numerical Recipes in Fortran, 2nd ed. (Cambridge University Press, 1992).
23. M.A. Lisa et al., Phys. Rev. C44 (1991) 2865.
24. Y.D. Kim et al., Phys. Rev. C45 (1992) 338.
25. D. Fox et al., Phys. Rev. C47 (1993) R421.
26. D.R. Bowman et al., Phys. Rev. Lett. (accepted).
27. T. Glasmacher, C.K. Gelbke, and S. Pratt, to be published.

Figures

FIG. 1: Matter distribution cuts along the $\hat{\mathbf{z}}$ and $\hat{\mathbf{y}}$ axes of the break-up geometries studied before Coulomb evolution: (a) spherical, (b) toroidal and (c) disk-shaped. The dimensions of the sources are indicated.

FIG. 2: Comparison of angle-integrated two-fragment ($3 \le Z \le 20$) correlation functions for the three different breakup geometries.

FIG. 3: Two-fragment ($3 \le Z \le 20$) correlation functions with the relative velocity of the two fragments parallel and transverse to the symmetry axis of a toroidal breakup configuration. The points in panel (a) were calculated assuming two-body Coulomb interaction between the two emitted fragments only. The calculations in panel (b) represent many-body trajectory calculations taking into account the Coulomb interactions between all emitted particles.

FIG. 4: Parallel ($|\hat{\mathbf{v}}_{rel} \cdot \hat{\mathbf{z}}| \ge 0.75$, open circles), transverse ($|\hat{\mathbf{v}}_{rel} \cdot \hat{\mathbf{z}}| \le 0.25$, filled circles), and angle-integrated two-fragment correlation functions (solid line) for (a) spherical, (b) toroidal and (c) disk-shaped breakup geometries constructed from light intermediate mass fragments ($3 \le Z \le 8$) selected by a cut on the direction of the total momentum of the fragment pairs corresponding to $|\hat{\mathbf{P}} \cdot \hat{\mathbf{z}}| \ge 0.75$. The statistical error bars are smaller than the symbols.

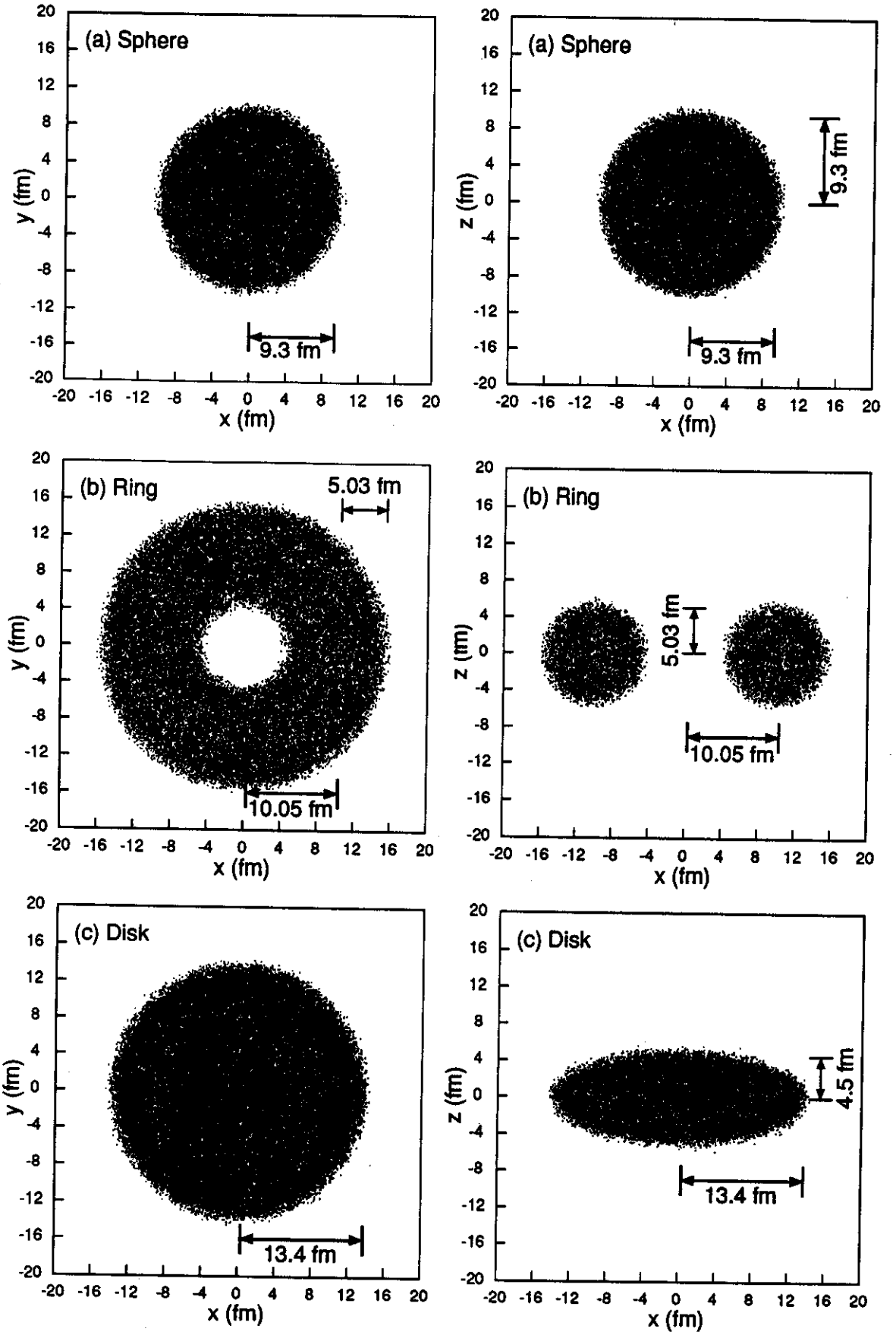

Glasmacher - Figure 1

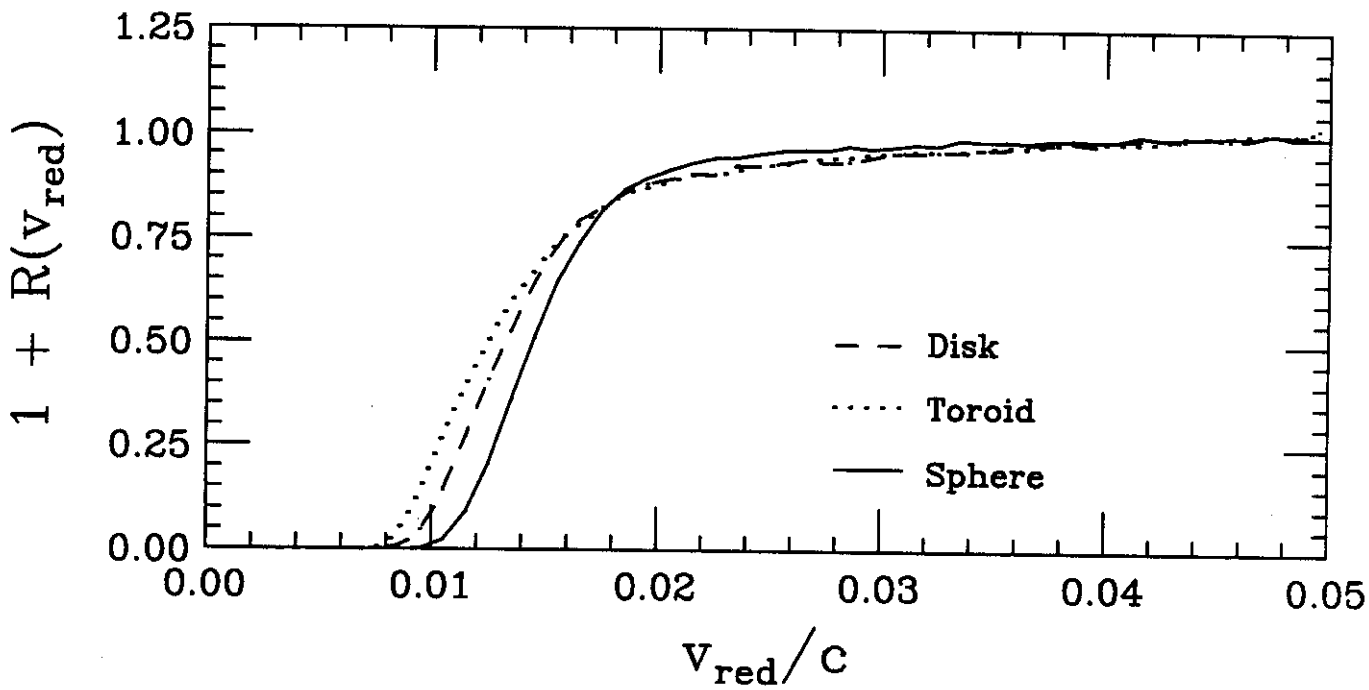

Glasmacher – PLB – Figure 2

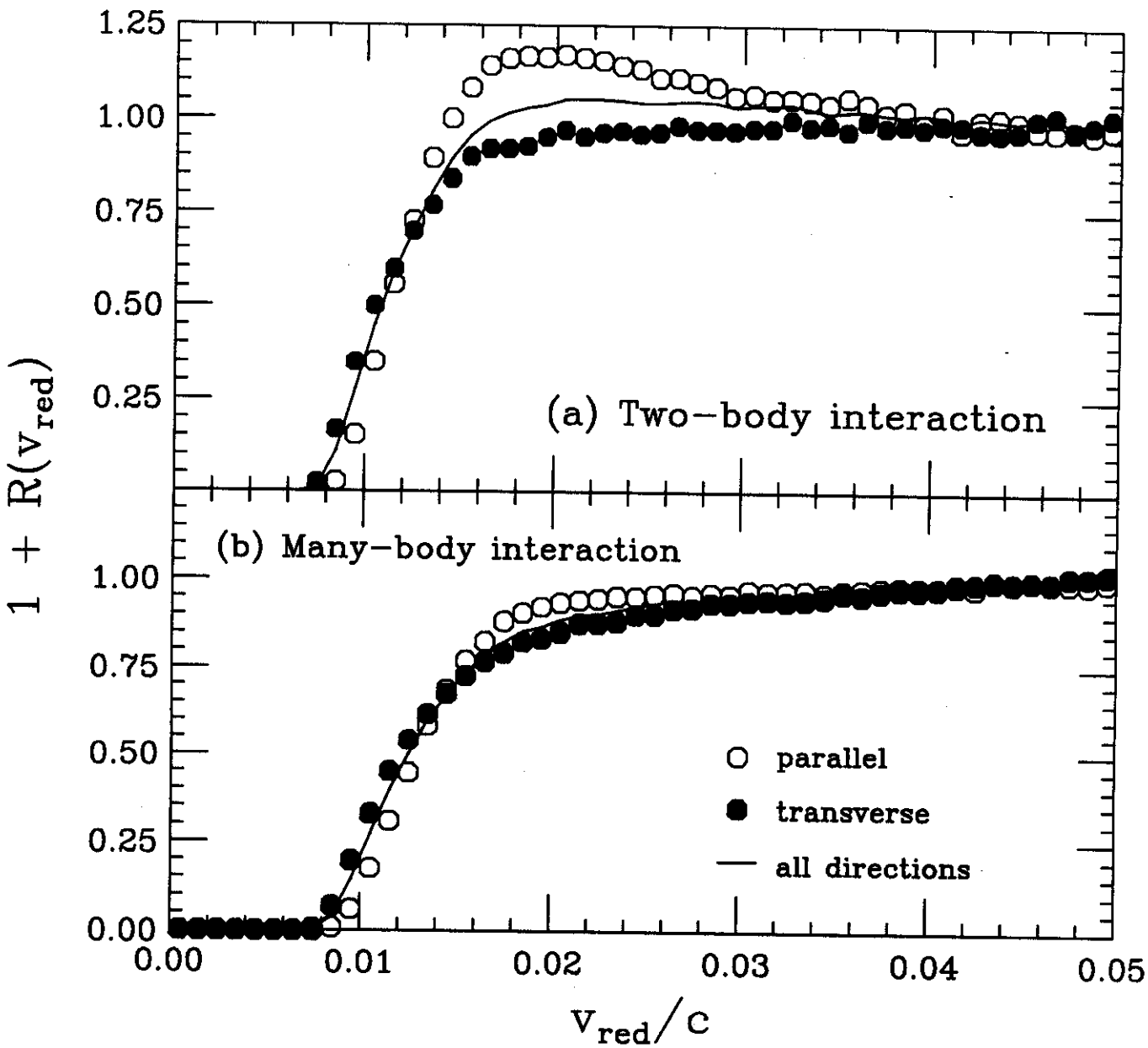

Glasmacher – PLB – Figure 3

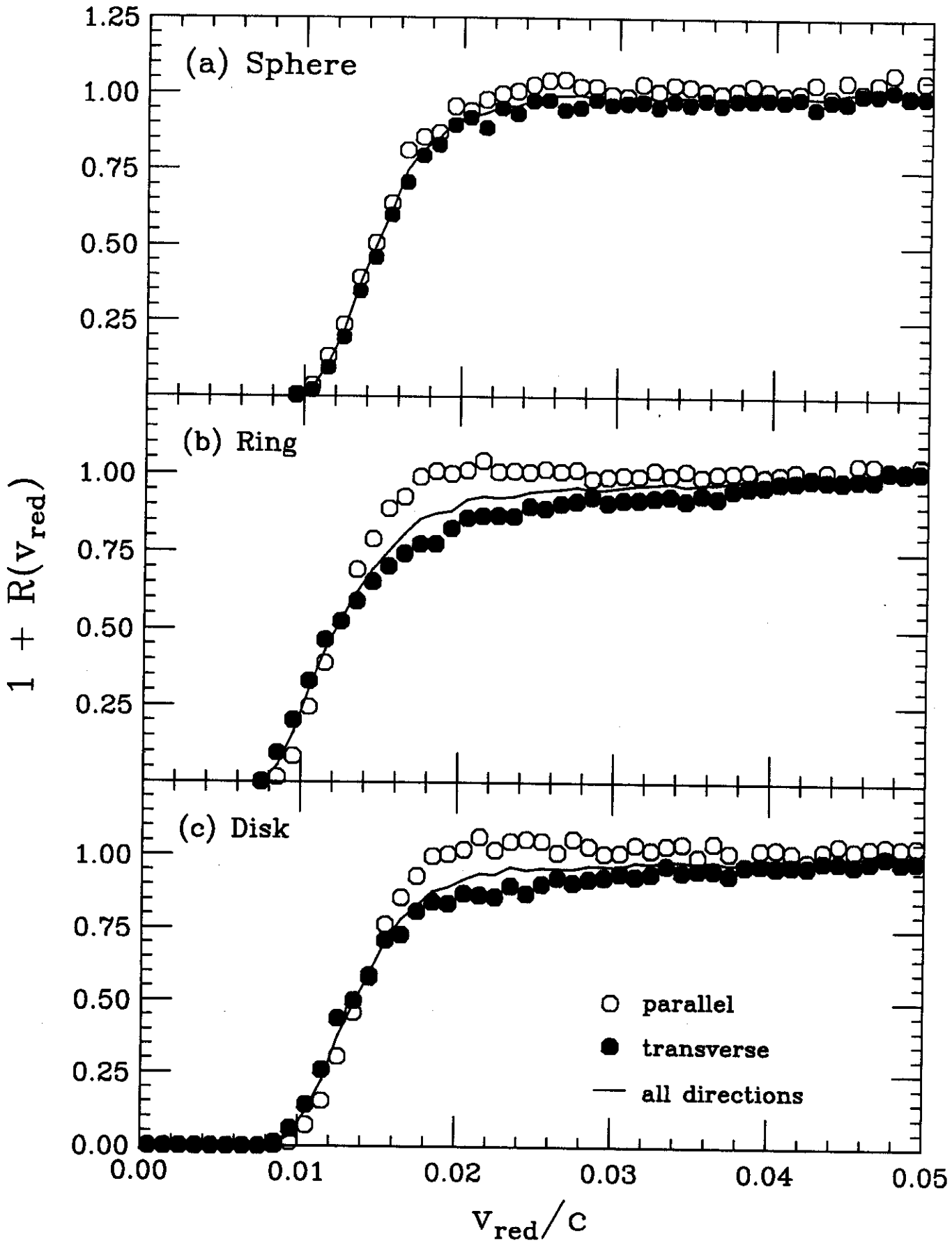

Glasmacher – PLB – Figure 4